Electronic Supplementary Material (ESI) for Physical Chemistry Chemical Physics.

Supplementary Material for "Electrokinetic Power Generation in Conical Nanochannels: Regulation Effects Due to Conicity"

Fang Qian, Wenyao Zhang, Deng Huang, Wenbo Li, Qiuwang Wang, Cunlu Zhao*

Key Laboratory of Thermo-Fluid Science and Engineering of MOE, School of Energy and Power Engineering, Xi'an Jiaotong University, Xi'an 710049, Shaanxi, China

*Corresponding author: mclzhao@xjtu.edu.cn

S1 Boundary conditions for governing equations

Fig.S1 shows the sketch of the simulation domain of the electrokinetic power generation system in Figure 2 in a two-dimensional cylindrical coordinate system $(r,\ z)$. Due to the axial symmetry, only half of the power generation system is simulated to reduce the computational load. The numerical simulation of electrokinetic power generation phenomena requires appropriate boundary conditions for the governing equations in the main text. Table S1 summarizes the boundary conditions for the Poisson equation, the Nernst-Planck (NP) equation and the Navier-Stokes (NS)/continuity equations.

For *the Poisson equation* which governs the electric potential distribution in the domain, the following boundary conditions apply: AH is the axis of the conical nanochannel consequently satisfies the symmetry condition; DE is the nanochannel wall which are negatively charged, and then is prescribed with a constant charge density boundary; BC and FG are the imaginary boundaries in two reservoirs located far away from the inlet and outlet of conical nanochannel, and therefore these two boundaries can be assumed to be in the bulk solution and are prescribed with zero charge density (i.e., n·$\overline{\nabla\psi}$=0); CD and EF are the solid walls of two reservoirs, and in this study are considered to be electrically neutral (i.e., n·$\overline{\nabla\psi}$=0) [1]; AB and GH can be the inlet or outlet boundary depending on the direction of applied pressure difference, and these two boundaries are provided with given potentials of $\overline{\psi}_l$ and $\overline{\psi}_r$, respectively. For the calculation of streaming potential in a forward pressure difference mode, we set $\overline{\psi}_l = 0$ (i.e., AB grounded), while $\overline{\psi}_r$ is self-constantly determined by satisfying the constraint of zero current $\overline{I} = 0$, and accordingly the streaming potential $\overline{\psi}_{st} = \overline{\psi}_r$. For the calculation of streaming potential in a backward pressure difference mode, we set $\overline{\psi}_r = 0$ (i.e., GH grounded), while $\overline{\psi}_l$ is self-constantly determined by satisfying the constraint of zero current $\overline{I} = 0$, and accordingly the streaming potential $\overline{\psi}_{st} = \overline{\psi}_l$. During the calculation of the current-voltage relationship, the electric potential on the non-grounded boundary varies from 0 to the streaming potential $\overline{\psi}_{st}$ with a step of 0.1 $\overline{\psi}_{st}$.

For *the NP equation* which governs the ion concentration, the following boundary conditions apply: AH is the axis of the conical nanochannel and consequently satisfies the symmetry condition; DE is the nanochannel wall and CD/FE are the walls of reservoirs, and these boundaries are prescribed with zero ion flux boundary ($n \cdot \overline{J}_\pm = 0$) because the solid walls are impervious to ions; BC and FG are imaginary boundaries of reservoirs and are considered to be impenetrable by ions, and thus zero ion flux boundary ($n \cdot \overline{J}_\pm = 0$) applies; AB and GH are prescribed with the bulk concentrations of cations and anions (e.g., $\overline{c}_+ = \overline{c}_- = 1$) since the reservoirs are large enough and these two boundaries are in the bulk electrolyte.

For *the NS and continuity equations* which govern the liquid flow and pressure distribution, the following boundary conditions apply: AH is the axis of the conical nanochannel consequently satisfies the symmetry condition; DE is the nanochannel wall and CD/EF are the walls of reservoirs, and these solid walls satisfy the no slip boundary condition $(i.e., \bar{u} = 0)$; BC and FG are prescribed with the slip boundary (equivalent to zero shear stress) because they are the imaginary boundaries in two reservoirs located far away from the inlet and outlet of conical nanochannel; AB and GH can be the inlet or outlet boundary depending on the direction of applied pressure difference, and these two boundaries are provided with given pressures of $\bar{p}_l$, and $\bar{p}_r$, respectively. For the forward pressure difference mode, we set $\bar{p}_l = \Delta p$, $\bar{p}_r = 0$, while for the backward pressure difference mode, we set $\bar{p}_l = 0$, $\bar{p}_r = \Delta p$.

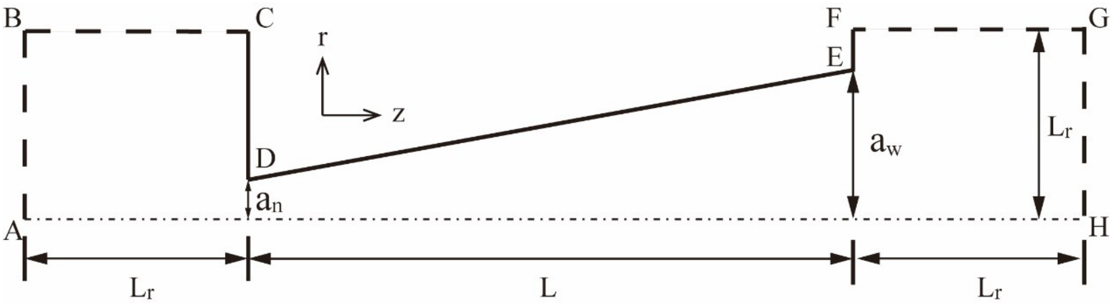

Figure S1. The 2D axisymmetric sketch of the simulation domain for the electrokinetic power generation system shown in Figure 2.

Table S1. Boundary conditions for the governing equations of the pressure-driven electrokinetic power generation

Boundary conditions	Poisson equation	NP equation	NS equation
AH (central axis)	Axial symmetry	Axial symmetry	Axial symmetry
AB (inlet/outlet)	$\bar{\psi}_l$	$\bar{c}_+ = \bar{c}_- = 1$	$\bar{p}_l$
GH (outlet/inlet)	$\bar{\psi}_r$	$\bar{c}_+ = \bar{c}_- = 1$	$\bar{p}_r$
BC, FG (imaginary boundaries)	$n \cdot \nabla\bar{\psi} = 0$	$n \cdot \bar{J}_\pm = 0$	$\bar{u} \cdot n = 0$
CD, EF (reservoir wall)	$n \cdot \overline{\nabla\psi} = 0$	$n \cdot \bar{J}_\pm = 0$	$\bar{u} = 0$
DE (nanochannel wall)	$n \cdot \overline{\nabla\psi} = -\bar{\sigma}$	$n \cdot \bar{J}_\pm = 0$	$\bar{u} = 0$

S2 Model validation

We solve the model numerically with the finite element software COMSOL Multiphysics 5.4, which features a capability of simulating the problem involving multiphysical processes as in this study. We use the mapped method to mesh the nanochannel domain with 230 elements and 3000 elements along the radial direction and the axial direction, respectively. Particularly, the element size in the radial direction decreases gradually by controlling the element ratio to create extremely fine mesh near the charged wall of the conical nanochannel. This is crucial for correctly capturing the dramatic change of ion concentration, velocity and electric potential in the EDL. The two reservoirs are meshed with the free triangular elements. We also notice that in order to obtain convergent results in the simulation the conical nanochannel requires more mesh elements than the nanochannel with uniform cross-section. By a mesh-independence study, we find that typically 690, 000 mapped elements in nanochannel and 26, 500 triangular elements in two reservoirs (a total of 716, 500 elements) lead to mesh-independent results.

To validate our model, we adopt the model to solve a benchmark case of the electrokinetic power generation in a nanochannel with uniform cross-section (e.g., b=1) under a low surface charge density condition, which has an analytical solution due to the Debye-Hückel approximation [2, 3]. Fig. S2 shows a comparison of the streaming potential obtained from the numerical solution and that obtained from the analytical solution. It is seen that our numerical model accords well with the analytical model for various channel sizes. Due to this fact, the current numerical model is robust and therefore ready for use to study the electrokinetic power generation in conical nanochannels.

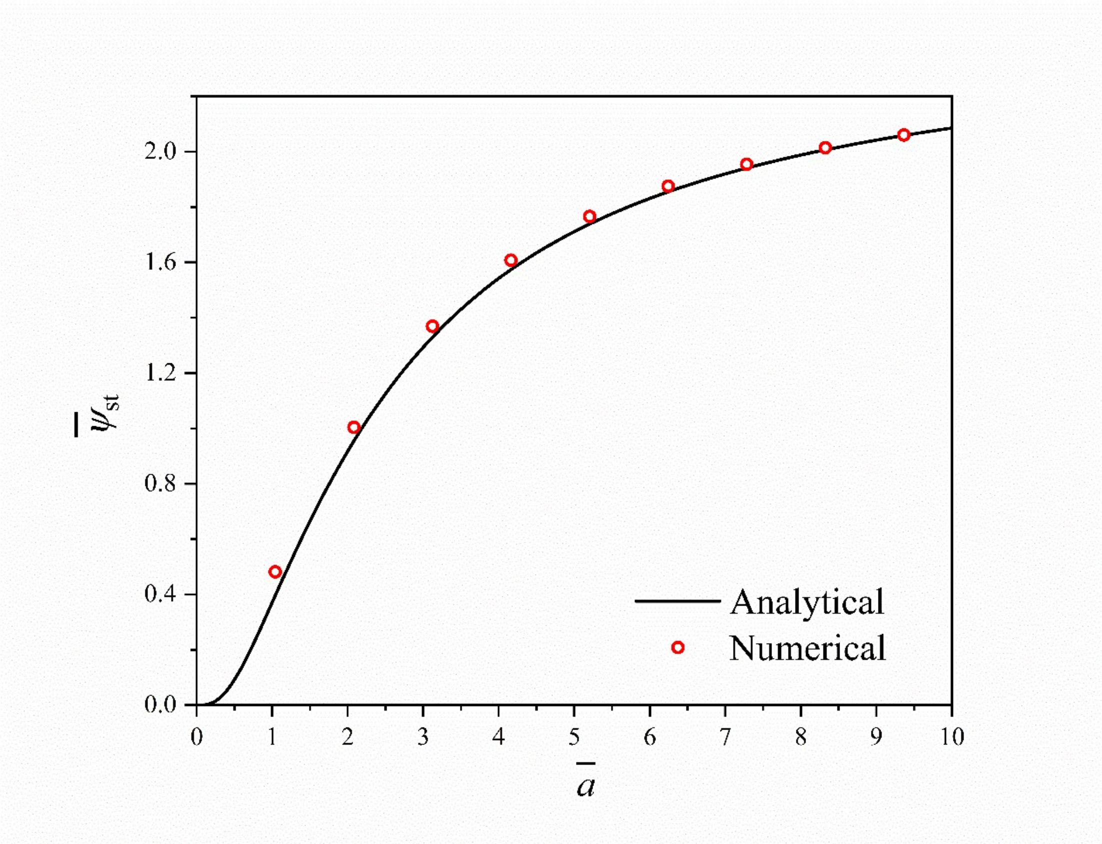

Figure S2. A comparison of the streaming potential obtained from our numerical model and that obtained from the analytical solution for a nanochannel of uniform cross-section with different values of scaled channel radius. In the calculations, the surface charge density $\overline{\sigma} =- 0.54$ and the pressure difference $\Delta\overline{p} = 20.18$.

S3 Radial ion concentration and electric potential distribution

Fig. S3 shows the radial ion concentration and electric potential profiles at three axial locations for the conicity of *b*=80. It is evident that with the increase of channel radius along the channel axis both cation and anion concentrations are able to achieve the bulk electrolyte concentration on the channel axis. This feature suggests the trend of EDL de-overlapping along the channel axis and the emergence of the electroneutral region at the wide end of the nanochannel. Meanwhile, the trend of EDL de-overlapping along the channel axis is also reflected by the flattening of the radial electric potential profiles.

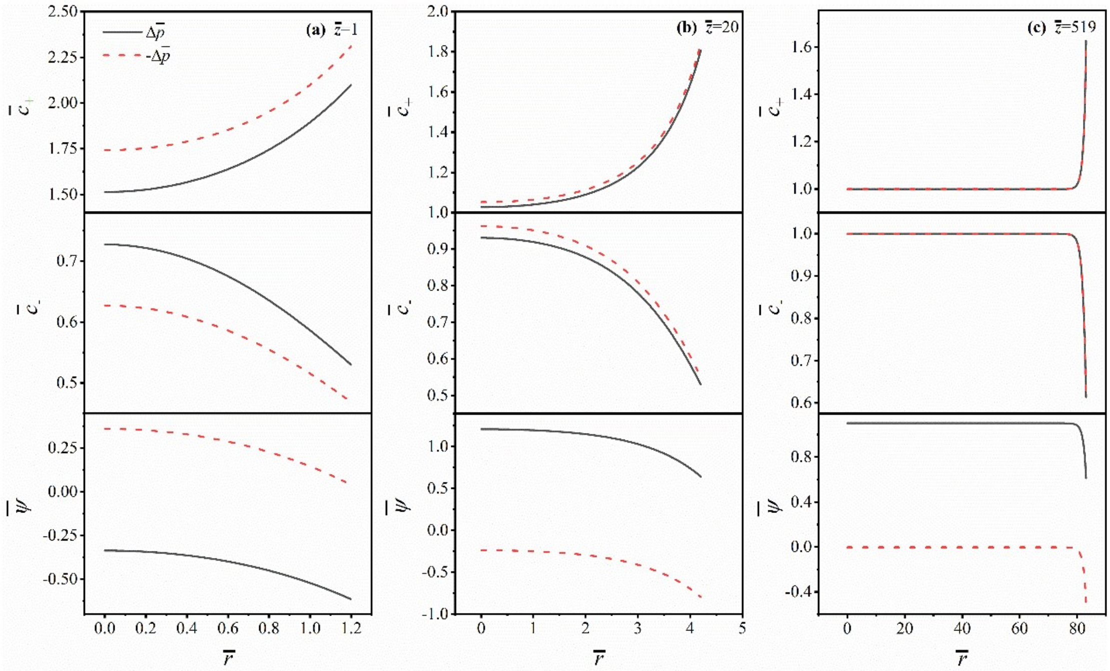

Figure S3. The steady-state radial profiles of cation concentration, anion concentration and electric potential for the conicity b=80 at three axial locations, namely, (a) $\bar{z} = 1$, (b) $\bar{z} = 20$, (c) $\bar{z} = 519$ under a forward (solid lines) and backward (dashed lines) pressure difference with the same magnitude of $|\Delta\bar{p}| = 100.9$ and a surface charge density of $\bar{\sigma} = -0.5$.

References

[1] H. Daiguji, P. Yang, A.J. Szeri, A. Majumdar, Nano Lett., 4 (2004) 2315-2321.

[2] J.H. Masliyah, S. Bhattacharjee, Electrokinetic and Colloid Transport Phenomena, John Wiley & Sons, Hoboken, 2006.

[3] F.H.J. van der Heyden, D. Stein, C. Dekker, Phys. Rev. Lett., 95 (2005) 116104.